Title:
CD226^{+} adipose tissue macrophages arise from MDP-derived monocytes and regulate lipid metabolism.

Authors:

Alexandre Gallerand[1]*, Zakariya Caillot[1], Marina Terekhova[2], Alexia Castiglione[1], Lorlana Leporati[1], Margaux Giacchero[1], Thomas Pilot[3], Michael Chang[4], Bastien Dolfi[1], Fairouz N. Zair[1], Eloïse Goës[1], Audrey Bennetot[1], Zandile Mlamla[5], Elvira Mass[6], Florent Ginhoux[7], David Voehringer[8], Matthias Mack[9], David Dombrowicz[10], Jesse W. Williams[4], David Masson[3], Maxim N. Artyomov[2], Adeline Bertola[1], Stoyan Ivanov[1]*

*equal contribution.

Affiliations:
1 Université Côte d'Azur, CNRS, LP2M, Nice, France.
2 Department of Pathology and Immunology, Washington University in St. Louis, School of Medicine, St. Louis, MO, USA.
3 Université Bourgogne Franche-Comté, LNC UMR1231, F-21000 Dijon, France.
4 Center for Immunology, Department of Integrative Biology and Physiology, University of Minnesota Medical School, Minneapolis, MN, USA.
5 Faculté de Médecine de Dijon, Diviomics (Plateforme de Lipidomique-uBourgogne), UMS Biosand, INSERM UMR1231, LabEx LipSTIC, UFR des Sciences de Santé de Dijon,France.
6 Developmental Biology of the Immune System, Life and Medical Sciences (LIMES) Institute, University of Bonn, Bonn, Germany.
7 Singapore Immunology Network (SIgN), Agency for Science, Technology and Research (A(∗)STAR), 8A Biomedical Grove, Immunos, Singapore 138648, Singapore; INSERM U1015, Gustave Roussy Cancer Campus, Villejuif 94800, France; Shanghai Institute of Immunology, Shanghai Jiao Tong University School of Medicine, Shanghai, China; Translational Immunology Institute, SingHealth Duke-NUS Academic Medical Centre, Singapore, Singapore.
8 Department of Infection Biology, University Hospital Erlangen and Profile Center Immunomedicine (i-MED) of the Friedrich-Alexander University Erlangen-Nuremberg (FAU), Erlangen, 91054, Germany.
9 Department of Nephrology, Regensburg University Medical Center, Regensburg 93042, Germany.
10 Univ.Lille, INSERM, CHU Lille, Institut Pasteur de Lille, U1011-EGID, 59000 Lille, France.

Correspondance to:
Stoyan.ivanov@univ-cotedazur.fr
Alexandre.gallerand@univ-cotedazur.fr

Abstract

Macrophages are innate immune cells present in all tissues, in which they participate in immune responses and maintenance of tissue homeostasis. They develop either from embryonic precursors or from circulating monocytes, and their functions are in part dictated by their origin. We previously observed robust monocyte recruitment and contribution to the macrophage pool in brown adipose tissue. In particular, monocytes were predicted to give rise to two phenotypically distinct macrophage subsets identifiable by CD206 or CD226 expression. In the present study, we investigated monocyte differentiation pathways in brown adipose tissue and the function of monocyte-derived macrophages. We found that bone marrow monocytes highly contributed to the CD226$^+$ macrophage population while the CD206$^+$ population contained mainly yolk sac-derived cells. Fate mapping analysis revealed a low contribution of GMP- and a high contribution of MDP-derived monocytes to the CD226$^+$ macrophage subset. Importantly, adoptive transfer experiments demonstrate that MDP- but not GMP-derived monocytes are pre-conditioned to give rise to CD226$^+$ macrophages. Using meta-analysis of single cell RNA-sequencing data, we found that MDP-derived CD226$^+$ macrophages were present in several tissues including peritoneal cavity, adrenal glands and all adipose depots, with a particular enrichment in beige and brown fat. A similar macrophage subset was identified in humans. Functionally, while depletion of CD206$^+$ macrophages using anti-CD115 blocking antibodies led to decreased adipose triglyceride content, genetic depletion of CD226$^+$ macrophages caused the opposite phenotype. We thus identify CD226$^+$ MDP-derived macrophages as a new myeloid cell type conserved across tissues and tied to lipid metabolism homeostasis.

Introduction

Macrophages are innate immune cells that have been observed in all organs (Mass et al., 2023). These cells originate from embryonic or bone marrow precursors (Ginhoux and Guilliams, 2016; Mass et al., 2023). In adulthood, the proportion of monocyte- and embryonically-derived macrophages varies in different tissues. Brain macrophages are derived from embryonic precursors and their pool is sustained through proliferation, while in gut, lung and spleen, macrophages are more frequently renewed by recruitment of blood monocytes (Ginhoux and Guilliams, 2016; Liu et al., 2019).

Brown adipose tissue (BAT) is actively involved in heat generation by adaptive thermogenesis (Rosen and Spiegelman, 2014). UCP1 (Uncoupling Protein 1) expression and high mitochondria content are BAT hallmarks (Nicholls, 2017). Previous work established that BAT contains several macrophage subsets that heavily rely on monocyte recruitment for their maintenance (Gallerand et al., 2021). Nevertheless, the functions of BAT macrophage subsets remain undefined. A subset of CX3CR1^{+} BAT macrophages regulates neuron network density and subsequently the thermogenic response (Wolf et al., 2017). Adipose tissue macrophage depletion with a CSF1R-blocking antibody was associated with a decreased local lipid content (Cox et al., 2021). Yet, whether this function is fulfilled by a selective macrophage subset, or requires the coordinated contribution of several macrophage populations, is not yet established.

Monocyte are generated in the bone marrow through a tight spatially and temporally regulated multistep process named myelopoiesis. Two major monocyte subsets are present in mice and express distinct phenotypic markers (Ingersoll et al., 2010; Sunderkotter et al., 2004). Ly6C^{high} classical monocytes are recruited to peripheral tissues at steady state and upon inflammation and contribute to the maintenance of tissue resident macrophages (Liu et al., 2019). Ly6C^{low} non-classical monocytes contribute to blood vessel health by secreting growth factors and play a pivotal role during cancer metastasis (Auffray et al., 2007; Carlin et al., 2013; Hanna et al., 2015). The majority of blood monocytes originate from a GMP-dependent precursor (Liu et al., 2019). However, an alternative pathway generating monocytes and dependent on MDPs has been also proposed (Menezes et al., 2016; Trzebanski et al., 2024). We previously established that BAT macrophages are constantly supplied by blood monocytes, yet whether GMP- and MDP-derived monocytes give rise preferentially or exclusively to selective BAT macrophage subsets is yet not established.

Results

CD226^{high} macrophages arise from monocytes but show low contribution from GMPs.

We recently demonstrated that BAT contained numerous immune cells by using single-cell RNA sequencing (scRNA-seq) analysis (Gallerand et al., 2021). Among those, myeloid cells were the most abundant populations (**Figure S1a**). BAT contained several monocyte, macrophage and dendritic cell (DC) clusters (**Figure S1a**). Among those cells, *Itgam* (CD11b) mRNA was expressed by the majority of the clusters (**Figure S1b**). We identified three monocyte subsets (clusters 2, 3 and 4) in BAT characterized by their relative expression of *Ly6c2* and *Nr4a1* mRNA (**Figure S1b**). Cluster 2 contained Ly6C^{low} monocytes and cluster 4 included Ly6C^{high} monocytes. Furthermore, we predicted that BAT contained 4 well-defined macrophage subsets (clusters 5, 6, 7 and 8). Cluster 5 macrophages expressed *Cd226* mRNA and several genes encoding for proteins involved in extracellular matrix remodeling and these

cells were named "Matrix" macrophages (**Figure S1c**) (Gallerand et al., 2021). Cluster 6 was the larger macrophage cluster (**Figure S1c**). Cluster 6 macrophages highly expressed genes previously associated with macrophage alternative polarization in response to IL-4 (*Mrc1*, *Lyve1*, *CD163*) (**Figure S1c**). These cells were called M2-like macrophages (**Figure S1c**) (Gallerand et al., 2021). Two additional macrophage clusters were also identified (clusters 7 and 8) and were characterized by the expression of enzymes involved in lipid metabolism (*Lpl* and *Plin2*). To validate at the protein level the predicted myeloid cell diversity in BAT, we developed a gating strategy and used spectral flow cytometry. Macrophages were identified as CD45$^+$ F4/80$^+$ MerTK$^+$ cells (**Figure 1a**). According to our scRNA-seq data predictions, matrix macrophages were found to highly express CD226 and had low CD64 (Fcgr1) expression (**Figures 1a, S1c and S1d**). M2-like macrophages were found to highly express CD206 and CD64 (**Figures 1a, S1c and S1d**). A fraction of these cells also co-expressed Lyve1 and Timd4, suggesting long tissue residency (**Figures 1a, S1c and S1d**). Uptake of intravenously injected TRITC-Dextran confirmed that CD206^{high} macrophages were associated to blood vessels while CD226^{high} macrophages showed lower dextran uptake (**Figure S1e**). We could not define distinct membrane markers for macrophage clusters 7 and 8, since these cells were identified as CD45$^+$ F4/80$^+$ MerTK$^+$ CD206$^-$ CD226$^-$ cells (DN macrophages). Monocytes were defined as CD45$^+$ MerTK$^-$ Ly6C$^+$ CD11b$^+$ Ly6G$^-$ cells (**Figure 1a**). We also found cells corresponding to conventional DC (cDC) subsets. cDC2 were identified as CD45$^+$ MerTK$^-$ CD11c$^+$ MHC-II$^+$ CD11b$^+$ cells while cDC1 were CD45$^+$ MerTK$^-$ CD11c$^+$ MHC-II$^+$ CD24$^+$ (**Figure 1a**).

Next, we aimed at defining the developmental connections between macrophage subsets. We previously demonstrated a high contribution of blood monocytes to the BAT macrophage pool (Gallerand et al., 2021). Using Slingshot analysis, we predicted that monocytes could generate two terminally differentiated BAT populations: matrix and M2-like macrophages (**Figure 1b**). Macrophage clusters 7 and 8 appeared as intermediate stages of differentiation towards the generation of clusters 5 and 6 (**Figure 1b**). Importantly, Timd4 expression was high selectively in the M2-like macrophages, suggesting that these cells could be, at least partially, from an embryonic origin (**Figure 1c**). Timd4 expression was low on DN and matrix macrophages further supporting their monocyte origin (**Figure 1c**). Our scRNA-seq data revealed that *Cx3cr1* mRNA was highly expressed in BAT monocytes but not macrophages (**Figure S1c**). To assess CX3CR1 protein expression on BAT myeloid cells, we used CXC3R1$^{GFP/+}$ mice (Jung et al., 2000). BAT monocytes and DN macrophages highly expressed CX3CR1 (**Figure 1d**). A fraction of M2-like macrophages (nearly 25%) was also GFP$^+$ (**Figure 1d**). GFP expression level was the lowest in BAT matrix macrophages (**Figure 1d**). These observations suggested that monocytes could differentially contribute to BAT macrophage subsets.

We next used genetic pulse-chase experiments to define monocyte contribution to BAT macrophage populations. CCR2^{CreERT2} X R26^{TdT} x CX3CR1$^{GFP/+}$ mice were administered with tamoxifen (TAM) and analyzed 48 hours later (**Figure 1e**). We investigated the appearance of TdTomato$^+$ cells in macrophage subsets and found that around 60% of CX3CR1^{GFP+} cells were labelled at this time point (**Figure 1e**). Importantly, the majority of CX3CR1-expressing CD206$^+$ BAT macrophages were not TdTomato$^+$, suggesting that this population is not monocyte-derived or its replenishment rate is slower in comparison to DN macrophages (**Figure 1e**). Among CX3CR1$^-$ BAT macrophages, TdTomato labelling was lower and around 12% were marked (**Figure 1e**). We noticed that CD206$^+$ M2-like macrophages were not labelled 48 hours after TAM administration, demonstrating low monocyte contribution to this macrophage population (**Figure 1e**). CX3CR1$^+$ cells thus appeared to be mostly monocyte-derived in BAT.

Next, we sought to establish the potential link existing between BAT CX3CR1^{+} and CX3CR1^{-} myeloid cells. We administered TAM in CX3CR1$^{CreERT2/GFP}$ x R26^{TdT} mice and followed TdTomato expression in BAT macrophages (**Figure 1f**). 2 days post-TAM administration, 66.6% of TdTomato^{+} BAT macrophages were CX3CR1^{GFP+} (**Figure 1f**). This percentage was lower 7 days after TAM, when the frequency of CX3CR1^{GFP+} macrophages among TdTomato^{+} cells was 33.8% (**Figure 1f**). This set of data demonstrated that CX3CR1 expression was rapidly decreased on BAT macrophages and suggested that the populations of CX3CR1^{-} BAT macrophages might still rely on monocyte recruitment for their maintenance.

To define the contribution of monocytes to BAT macrophage subsets, we treated mice with anti-CCR2 MC-21 antibody allowing to efficiently deplete monocytes (Mack et al., 2001). In BAT, we observed an almost complete monocyte depletion 24 hours after MC-21 treatment, in comparison to control animals (**Figure 1g**). Thus, we investigated the consequence of monocyte depletion on BAT macrophage subset dynamics. Continuous MC-21 administration kept monocytes absent from BAT over time (**Figure 1h**). DN macrophage numbers tended to decrease as well, while matrix macrophages tended to augment at 24 hours post MC-21 injection (**Figure 1h**). This observation is in line with the non-association of matrix macrophages with blood vessels (**Figure S1e**), that could prevent direct MC-21 binding on these cells. Monocytes, DN and matrix macrophages were all decreased at 2 and 5 days of MC-21 treatment (**Figure 1h**). These data indicated that DN macrophages strongly depend on monocyte flux to sustain constant numbers while depletion of matrix macrophages was slower (**Figure 1h**).

To track monocyte differentiation into BAT macrophage subsets we used Ms4a3$^{Cre/ERT2}$ x R26^{TdT} mice (Liu et al., 2019). Mice were gavaged with TAM and the frequency of TdTomato^{+} cells in each macrophage subset was defined in a time-course manner. As previously described (Liu et al., 2019), we observed that blood monocyte labelling efficiency reached 90-95% (**data not shown**). 3 days after the last TAM administration, around 70% of BAT monocytes were TdTomato^{+} (**Figure 1i**). This percentage rapidly decreased and at day 17 we observed the disappearance of TdTomato^{+} monocytes in BAT due to their replacement by unlabeled bone marrow-derived monocytes (**Figure 1i**). The labelling of DN BAT macrophages peaked at day 3, when 20% of cells were labelled, further supporting that this population depended on monocytes to sustain (**Figure 1i**). Of interest, the labelling of BAT matrix macrophages peaked at day 10 when labeling of DN macrophages was decreasing (**Figure 1i**). This demonstrated that while matrix macrophages rely at least partially on monocytes for their maintenance, their differentiation trajectory occurs over a longer time frame. We detected very low contribution (less than 3%) of GMP-derived blood monocytes to BAT M2-like macrophages (**data not shown**). Finally, and to define the maximal contribution of GMP-derived monocytes to BAT macrophages, we investigated the frequency of TdTomato^{+} cells in 6-week-old Ms4a3^{Cre} x R26^{TdT} mice. In this genetic model, we observed that 80% of BAT monocytes were TdTomato+ (**Figure 1j**). In agreement with our previous observation, around 60% of BAT DN macrophages were also labelled (**Figure 1j**). We also found that 40% of BAT M2-like macrophages were generated by GMP-derived monocytes, demonstrating that monocytes contribute to the pool of these cells (**Figure 1j**). Surprisingly, the lowest labeling was observed in BAT matrix macrophages, where only around 25% of cells were TdTomato^{+} (**Figure 1j**). These data indicated that while blood monocytes massively contributed to BAT matrix macrophage maintenance, only 25% of these cells originated from a GMP-derived progenitor.

We previously demonstrated that BAT expansion heavily relied on monocyte recruitment and their differentiation into macrophages (Gallerand et al., 2021). Aging is associated with BAT expansion and "whitening". Thus, we decided to analyze BAT macrophage diversity throughout life in female and male mice. Macrophage frequency increased with age and this phenotype was dominated by an accumulation of M2-like macrophages (**Figure S2A**). The relative abundance of DN and matrix BAT macrophages remained similar in young and old mice (**Figure S2A**). However, in a genetic model of BAT expansion (Ucp1^{Cre} x Pnpla2$^{fl/fl}$ mice), we documented increased numbers of M2-like, matrix and DN macrophages (**Figure S2B**). Thus, depending on the model being analyzed, BAT macrophage subsets displayed a drastically different behavior during tissue expansion.

CD226^{high} macrophages are conserved across tissues and enriched in thermogenic adipose depots.

We next sought to define whether macrophages with characteristics similar to BAT matrix macrophages exist in other tissues. Small peritoneal cavity macrophages (SCMs) were demonstrated to express CD226 and to heavily rely on monocytes for their maintenance (Kim et al., 2016). These cells reside in the peritoneal cavity where they share the local microenvironment with large peritoneal macrophages (LPMs). LPMs and SCMs, despite living in the very same environment, display specific transcriptional signatures (Immgen dataset) (**Figure 2a**). We compared these the transcriptomic profile of BAT matrix macrophages to that of peritoneal LPMs and SCMs, and found that they strongly resembled SCMs (**Figure 2a**), indicating that the CD226^{+} macrophage subset could be conserved across several tissues.

Interestingly, we observed that a myeloid cluster also expressed CD226 in our previously published single cell RNA-sequencing dataset of adrenal gland (AG) immune cells (Dolfi et al., 2022). A recent direct comparison between murine and human peritoneal cavity immune cells revealed that CD226^{+} SCMs are conserved in humans and show similarities with human type 2 dendritic cells (Han et al., 2024). Based on these observations, we aimed to decipher (i) whether CD226^{+} macrophages were present in other tissues beyond BAT and peritoneal cavity and (ii) whether these cells might share part of their signature with dendritic cells. To answer these questions, we integrated myeloid cells from previously published scRNA-seq datasets from BAT (Gallerand et al., 2021), AG (Dolfi et al., 2022) and peritoneal cavity (Han et al., 2024), as well as splenic Flt3^{+} cells containing plasmacytoid and conventional (type 1, 2 and 3) dendritic cells (Liu et al., 2023) (**Figure 2b**). CD226^{+} macrophages were identified in BAT, AG and peritoneum but not spleen (**Figure 2b**) and they clustered together (**Figure 2c**). Importantly, CD226^{+} cells clustered away from recently-described type 3 dendritic cells (cDC3) that express markers common with the macrophage lineage including CD16/32 and CD115 (Liu et al., 2023) (**Figure 2c**). Indeed, CD226^{+} macrophages lacked expression of the core signature of cDC3 (**Figure 2d**). We next explored a publicly available dataset generated by the Tabula muris consortium (Tabula Muris, 2020) to test whether CD226^{+} macrophages could be found in additional tissues. We generated a gene set named "CD226^{high} signature", comprising the 50 genes with highest differential expression between BAT CD226^{+} macrophages and other BAT immune cells. This signature was absent in most of the dataset, except for one group of cells (**Figure S3a, left**). Indeed, cells highly expressing this gene set clustered together (**Figure S3a, right**). These cells were predicted to be myeloid cells and in particular macrophages (**Figure S3b**). They were enriched in adipose tissue and limb muscle, even though they were also detected at a lower degree in heart, trachea and mammary glands (**Figure S3b**). In agreement with our data presented in

Figure S2a, the abundance of CD226$^+$ macrophages did not depend on biological sex nor age (**Figure S3b**).

Next, we generated a genetic model to target and track CD226$^+$ macrophages across tissues. Resistin like alpha (*Retnla*) appeared to be a hallmark gene for both BAT and peritoneal CD226$^+$ macrophages (Gallerand et al., 2021; Kim et al., 2016). We could confirm that *Retnla* expression was highly expressed in CD226$^+$ macrophages in our integrated dataset (**Figure 2e**). Thus, we crossed Retnla^{Cre} mice (Krljanac et al., 2019) with R26^{TdT} reporter animals. In these mice, TdTomato expression was exclusively detected in CD45$^+$ cells in BAT (**Figure 2f**). Among CD45$^+$ cells, TdTomato expression was highly enriched in myeloid (F4/80$^+$) cells (**Figure 2f**). Among BAT macrophages, the highest TdTomato expression was detected in matrix macrophages, although lower labelling was also detected in BAT M2-like and DN macrophages (**Figure 2f**). Blood monocytes were not labeled with TdTomato (**Figure 2f**). In the peritoneal cavity, we could confirm that TdTomato was expressed by SCMs but not by dendritic cells (**Figure S3c**). We next investigated the presence of CD226$^+$ macrophages in different adipose tissue depots and compared brown (BAT, periaortic AT (PeriAo)), beige (subcutaneous (SCAT) and perirenal (PeriRen) AT) and white (pericardiac AT (PeriCard), omentum and WAT) fat, all associated with different thermogenic capacity (**Figure S3d**). While CD226$^+$ macrophages were detected in all the aforementioned tissues, their relative frequency was increased within tissues with high thermogenic potential (**Figure 2g**). Furthermore, these cells were efficiently labelled in Retnla^{Cre} R26^{TdT} mice (**Figure 2g**).

Together, our data indicate that CD226^{high} Retnla$^+$ myeloid cells are a unique macrophage subset that is conserved across tissues and enriched in thermogenic adipose depots.

CD226^{high} macrophages arise mainly from MDP-derived monocytes.

Despite the clear contribution of blood monocytes to BAT CD226$^+$ macrophages, only a small fraction of these cells was labelled in Ms4a3^{Cre} R26^{TdT} mice (**Figure 1j**). SCM labelling reached similar level, while 95% of blood monocytes were TdTomato$^+$ (**Figure 3a**). Recently, it was demonstrated that a proportion of blood monocytes arise from a GMP-independent and MDP-dependent precursor (Trzebanski et al., 2024). However, these observations relied on scRNA-seq data and adoptive transfer experiments, and genetic tools allowing to track MDPs and their progeny are lacking. We thus used RNA sequencing data from the Immgen consortium to compare GMPs to MDPs and identify subset-specific genes that could be targeted using existing genetic tools (**Figure S4a**). *Flt3* and *Ccr2* were present among the 30 most differentially expressed genes, however blood monocytes can be highly labeled using Flt3^{Cre} and Ccr2^{Cre} mice due to expression of these genes upstream and downstream of monocyte progenitors, making them incompatible with progenitor-restricted fate mapping. However, we identified *Clec9a* as a gene with higher expression in MDPs compared to GMPs (**Figure S4a**). Indeed, *Clec9a* appeared to be expressed in MDPs and CDPs but not in upstream progenitors nor GMPs and monocytes (**Figure 3b**). We thus crossed Clec9a^{iCre} mice (Schraml et al., 2013) to R26^{TdT} mice and analyzed bone marrow progenitor labelling efficiency (**Figure S4b**). Our data revealed that 40% of CDPs and 10% of MDPs were TdTomato$^+$ (**Figure 3c**). cMoPs were not labelled and remained TdTomato$^-$ (**Figure 3c**). We also detected a population of bone marrow monocytes (around 5%) that expressed TdTomato (**Figure 3c**). These data indicated that Clec9a labelling in monocytes could reflect a MDP-dependent origin.

We next analyzed the presence of TdTomato$^+$ cells in peripheral blood immune cell populations (**Figure S4c**). Our data demonstrated that around 5% of blood monocytes were

labelled in Clec9a^{iCre} R26^{TdT} mice (**Figure 3d**), mirroring blood monocyte labeling using Ms4a3^{Cre} mice. Equal TdTomato labeling was observed in Ly6C^{high} and Ly6C^{low} blood monocytes (**Figure 3d**). However, no additional blood immune cells were labelled. Indeed, neutrophils, B and T cells (both CD4^{+} and CD8^{+} subsets), Natural Killer (NK) cells remained TdTomato^{-} (**Figure S4d**). While blood monocyte labelling ranged around 5-10%, a higher percentage of TdTomato^{+} monocytes was detected in peritoneal and BAT monocytes (**Figure 3e**). The majority (70-80%) of BAT and peritoneal CD226^{+} macrophages were also labelled (**Figure 3e**). These data mirrored the labelling percentage documented in Ms4a3^{Cre} R26^{TdT} mice. Only a small fraction of LCMs was TdTomato^{+} in Clec9a^{iCre} R26^{TdT} mice (**Figure 3e**). We confirmed that this was not due to Clec9a mRNA expression in SCMs (**Figure S4e**) nor BAT CD226^{high} macrophages (**Figure S4f**). Taken together, these data suggested that MDP-derived monocytes are enriched in peritoneal cavity and BAT among CD226^{+} macrophages.

Based on the observation that MDP-derived monocytes had a higher contribution to CD226^{high} macrophages than GMP-derived monocytes across tissues, we hypothesized that monocyte differentiation trajectories were pre-conditioned by monocyte origin. To test this hypothesis, we cell-sorted total splenic monocytes from Clec9a^{iCre} R26^{TdT} mice (CD45.2^{+} cells) and transferred them intraperitoneally in CD45.1 host mice without prior treatment (**Figure 3f**). 7 days after injection, the presence and phenotype of donor CD45.2 cells were analyzed by flow cytometry. We observed that TdTomato^{-} donor cells preferentially gave rise to LPMs (**Figure 3f and 3g**). In striking contrast, TdTomato^{+} cells generated both CD226^{+} SCMs and LPMs (**Figure 3f and 3g**). Despite the fact that only ~7% of donor cells were TdTomato^{+} (**Figure 3f**), 60% of donor CD226^{+} SCMs were TdTomato^{+} (**Figure 3g**). These results demonstrate that monocyte origin dictates their ability to generate specific tissue resident macrophage subsets.

CD226^{high} adipose tissue macrophages regulate lipid metabolism.

Finally, we aimed to explore the functions of CD226^{+} macrophages. First, we treated mice with a CSF1R blocking Ab (clone AFS98). Mouse body weight and BAT weight tended to decrease in AFS98-injected mice in comparison to isotype controls (**Figure S5a**). In BAT, AFS98 administration did not induce a complete macrophage depletion (**Figure 4a**). Indeed, a significant proportion of BAT macrophages remained present in AFS98-treated mice (**Figure 4a**). AFS98 administration decreased the number of BAT M2-like macrophages (**Figures 4b and 4c**). We also noticed a similar trend for DN and matrix macrophages while it did not reach a statistical significance (**Figure 4c**). Thus, BAT M2-like macrophages were the population with the highest dependence on CSF1R signaling. AFS98 triggered a well-defined morphological change in BAT with diminished presence of adipocytes with large lipid droplets in comparison to control treated animals (**Figure 4d**). Lipidomic analyses demonstrated that BAT triglyceride (TG) content was decreased in AFS98 injected mice (**Figure 4e**). Of note, serum TG levels remained similar between both groups of animals (**Figure S5b**). Free fatty acids concentration and diversity were not modified by AFS98 administration (**Figure S5c**). These results indicate that CD206^{high} macrophages could support triglyceride storage in BAT, a finding in agreement with recently published results in WAT (Cox et al., 2021).

We next investigated the role of CD226^{+} macrophages on BAT lipid content. We generated Retnla^{Cre} R26^{DTA} mice (Retnla^{DTA}) to deplete CD226^{+} macrophages across tissues. Blood immune cells were not affected in these mice, indicating the absence of systemic inflammation (**Figure S5d**). However, we observed an almost complete absence of BAT Matrix macrophages (**Figure 4f**). Importantly, M2-like and DN BAT macrophage numbers remained similar between control and Retnla^{DTA} animals (**Figure 4g**). We also noticed the disappearance

of CD226$^+$ macrophages in all adipose tissue depots that we analyzed (**Figure S5e)**. We also noticed a complete disappearance of SCMs in the peritoneal cavity while LCMs were not affected (**Figure S5f**). Other immune cell types were also unaffected in BAT (**Figure S5g**). Retnla^{DTA} mice are thus appropriate tools to address the function of CD226$^+$ macrophages.

Depletion of CD226$^+$ macrophages triggered a specific BAT phenotype characterized by increased adipocyte droplet size (**Figure 4h**). This was associated with an increased total BAT TG content in Retnla^{DTA} mice when compared to littermate controls, with a particular enrichment of long-chain TGs (**Figure 4i**). We did not detect changes in serum non esterified fatty acids (NEFA) and glucose levels in Retnla^{DTA} mice (**Figure S5h**). However, their serum TG levels were higher than controls while their glycerol levels trended downwards (**Figure 4j**), indicating that CD226$^+$ macrophages were regulating triglyceride metabolism.

Discussion

In the present study, using genetic fate mapping, we demonstrated that a population of blood monocytes is generated independently of GMP-derived cells. We found that these cells are efficiently labelled in Clec9a^{iCre} R26^{TdT} mice suggesting that those monocytes arise mainly from MDPs. Of note, these monocytes preferentially generated CD226$^+$ macrophages in adipose tissue and peritoneal cavity, demonstrating the monocyte origin influences their fate. Whether other macrophage subsets also arise mainly from MDPs remains to be established. While the phenotypic distinction between monocytes, macrophages and DCs was challenging for a long time, key findings reported in 2012 by the Immgen consortium solved this problem (Gautier et al., 2012; Miller et al., 2012). Macrophages were defined as CD64$^+$MerTK$^+$ cells, markers that were not expressed on conventional DCs (Gautier et al., 2012). We found that CD226$^+$ macrophages across tissues displayed a low CD64 expression, challenging the current classification of cells in the macrophage or DC lineage based on these criteria. While BAT CD226$^+$ macrophages expressed MerTK and F4/80, supporting their macrophage identity, they also expressed CD11c and MHC-II, two markers traditionally detected and associated with DCs. A key feature of DCs, that is not shared with tissue resident macrophages, is their ability to migrate through the lymphatic vessels to local draining lymph nodes (Randolph et al., 2017). DC migration via the lymphatic endothelial system depends on a single chemokine receptor, CCR7. Indeed, CCR7 expression allows to discriminate between DCs and macrophages. CD226$^+$ macrophages lack CCR7 expression (data not shown), thus suggesting that these cells cannot migrate through the lymphatic vessels. Furthermore, our data revealed that GMP- and MDP-derived monocytes contribute both to the generation of CD226$^+$ macrophages. Therefore, one could expect that depending on their origin, GMP- and MDP-derived CD226$^+$ macrophages could display selective functions. Their high MHC-II expression suggests a role in antigen presentation and initiation of adaptive immunity. The ability of GMP- and MDP-derived CD226$^+$ macrophages to trigger a T cell response remains to be established.

Previous work on SCMs demonstrated that these cells rely on the transcription factor IRF4 (Kim et al., 2016). This study indicated that, independently of their origin, SCMs rely on a unique transcription factor for their survival. However, while only 5% of blood monocytes originate from MDPs, 70% of SCMs arose from these monocytes. Monocytes rely on the chemokine receptor CCR2 for their bone marrow egress and tissue entry (Serbina and Pamer, 2006). While SCM numbers are reduced in CCR2-deficient mice (Kim et al., 2016), they are

not fully abolished. One could wonder whether MDP-derived monocytes rely solely on CCR2 for bone marrow egress and their subsequent tissue recruitment. Mechanisms governing MDP-derived monocyte bone marrow retention and egress thus require further investigations that are beyond the focus of the present study.

We observed a conserved ratio of Ly6C^{high} : Ly6C^{low} monocytes independently of their origin, suggesting that monocyte conversion occurs at a similar rate in GMP- and MDP-derived monocytes. Yet, our data indicates that GMP- and MDP-derived monocyte fate in tissues depends on their lineage. MDP-derived monocytes are preferentially recruited to specific tissues, i.e. adipose tissues and limb muscle where CD226^{+} macrophages are enriched. A recent study demonstrated that monocytes locally proliferate upon their tissue recruitment before giving rise to tissue resident macrophage subsets (Vanneste et al., 2023). The proliferative rate of GMP- and MDP-derived monocytes could be significantly different, and this might explain, at least partially, their ability to differentially contribute to specific tissue resident macrophage subsets. The lifespan of GMP- and MDP-derived CD226^{+} macrophages could be an additional factor involved in the aforementioned process.

CD226^{+} macrophages were enriched in adipose tissue and in particular thermogenic depots. Depletion of CD226^{+} macrophages was associated with an increased local and systemic TG content, demonstrating a central role of these cells in lipid metabolism. While CD226^{+} macrophages express several enzymes involved in lipid metabolism (Gallerand et al., 2021), how precisely these cells control local and systemic TG content requires further investigations. Previous reports demonstrated that adipose tissue macrophages control lipid storage in a PDGFcc-dependent manner (Cox et al., 2021). Of note, mice treated with anti-CSF1R blocking antibody and CCR2$^{-/-}$ mice displayed a different behavior when challenged with high fat diet (Cox et al., 2021). While both CD206^{high} and CD226^{high} macrophages show CCR2-dependent monocyte contribution (Figure 1) (Gallerand et al., 2021), monocytes mainly contribute to the DN and CD226^{high} subsets. Our data demonstrated that adipose tissue CD206^{+} macrophages showed a higher CSF1R dependence in comparison to DN and CD226^{+} macrophages. Using our single cell RNA-sequencing data, we could determine that *Csf1r* expression is higher in CD206^{high} macrophages compared to the CD226^{high} population (data not shown), which could explain the differential impact of AFS98 administration between these two subsets. Whether GMP- and MDP-derived CD226^{+} macrophages rely to a similar extent on CSF1R signaling for their proliferation and renewal needs to be defined. Inversely, CD226^{high} macrophages expressed high levels of *Csf2ra* mRNA compared to CD206^{high} macrophages (data not shown). This observation suggests that GM-CSF signaling plays a role in the maintenance of CD226^{high} macrophages.

In the present study, we identify CD226^{+} macrophages as a new myeloid subset bearing features of both macrophages (F4/80^{+} MerTK^{+}) and dendritic cells (CD64^{low} CD11c^{+} MHC-II^{high}), that is conserved across tissues. Similar findings were reported in a recent study comparing murine and human peritoneal cells (Han et al., 2024). Indeed, the human counterpart to murine CD226^{+} SCMs appeared to be CD14^{+} cells that also express the DC marker CD1c (Han et al., 2024). Importantly, this observation indicates that CD226^{+} cells described herein are conserved in humans. We detected a similar population in human white adipose tissue (Human Single Cell Atlas from the Broad Institute, data not shown), indicating that these cells are also conserved across several tissues in humans. This work paves to way to define the relative role of GMP- and MDP-derived monocytes during infections, acute and chronic (obesity, atherosclerosis…) inflammatory diseases and cancer development.

Acknowledgments

We would like to thank the C3M Animal facility for technical support and the GIS-IBISA multi-sites platform Microscopie Imagerie Côte d'Azur (MICA), and particularly the imaging site of C3M (INSERM U1065) supported by Conseil Régional, Conseil Départemental, and IBISA. We would also like to thank the C3M Flow Cytometry Core Facility financed by Conseil Général CG06 and Conseil Régional PACA. SI is funded by Institut National de la Sante et de la Recherche Medicale (INSERM) and Agence Nationale de la Recherche (ANR-22-CE14-0027-02; ANR-21-CE15-0020-02; ANR-23-CE14-0054-02; ANR-23-CE15-0032-01). JWW was supported by NIH R01AI165553. AG was supported by the French government through the UCAJedi Investments in the Future projects managed by the National Research Agency (ANR) (ANR-15-IDEX-01). EM was funded by the Deutsche Forschungsgemeinschaft (DFG, German Research Foundation) under Germany's Excellence Strategy-EXC2151-390873048, SFB1454 (Project number 432325352), and FOR5547 – Project-ID 503306912.

Author contribution

AG and SI designed the study. AG and SI wrote the manuscript and prepared the figures with input from all co-authors. AG, ZC, MT, AC, LL, MG, BD, EG, ZM, FNZ, MC, TP, AB, JWW, AB and SI performed experiments. AG, ZC, MT, AC, LL, MG, TP, JWW, DM, MNA, AB and SI analyzed data. EM, FG, DV, MM and DD provided tools and expertise. SI obtained funding for the project.

Conflicts of interest

The authors declare no competing interests.

Methods

Experimental models

Mouse models

Wild-type C57BL/6J (Jax #000664), CX3CR1^{gfp} (B6.Cg-Ptprca Cx3cr1$^{tm1Litt/LittJ}$, Jax #008451), Ms4a3^{cre} (C57BL/6J-Ms4a3$^{em2(cre)Fgnx}$/J, Jax #036382), R26$^{LSL\text{-}TdTomato}$ (B6.Cg-Gt(ROSA)26Sor$^{tm9(CAG\text{-}tdTomato)Hze}$/J, Jax#007909), Clec9a^{icre} (B6J.B6N(Cg)-Clec9a$^{tm2.1(icre)Crs}$/J, Jax#025523), Pnpla2$^{fl/fl}$ (B6N.129S-Pnpla2^{tm1Eek}/J, Jax#027278), UCP1^{cre} (B6.FVB-Tg(Ucp1-cre)1Evdr/J, Jax#024670), CD45.1 (B6.SJL-Ptprc^{a} Pepc^{b}/BoyJ, Jax# 002014) and R26$^{LSL\text{-}DTA}$ (B6.129P2-Gt(ROSA)26Sor$^{tm1(DTA)Lky}$/J, Jax# 009669) mice used in this study were maintained under C57BL/6J background and originally purchased from Jax Labs. CCR2$^{cre/ERT2}$ (C57BL/6NTac-Ccr2$^{tm2982(T2A\text{-}Cre7ESR1\text{-}T2A\text{-}mKate2}$) mice. (Croxford et al., 2015) were provided by Dr. Burkhard Becher. Ms4a3$^{cre/ERT2}$ mice (Liu et al., 2019) were provided by Dr. Florent Ginhoux. Retnla^{cre} mice (Krljanac et al., 2019) were provided by Dr. David Voehringer. Experimental and control animals were co-housed, and littermate controls were used as often as possible. All mice were bred and housed in specific pathogen-free conditions maintained in facilities in the Mediterranean Center of Molecular Medicine (INSERM U1065, Université Côte d'Azur), Washington University in Saint Louis animal facility or the University of Minnesota Medical School Research Animal Resources facility. An ambient temperature of ~20-23 °C was maintained, with a 12/12-hour light/dark cycle and food available ad libitum. Animals were euthanized by cervical dislocation. Animal protocols required for experimentation other than organ collection were authorized by the French Ministry of Higher Education and Research upon approval of the local ethical committee (CIEPAL Azur) at

Université Côte d'Azur, and by the Institutional Animal Care and Use Committee (IACUC) at University of Minnesota Medical School.

***In vivo* treatments**

Administration of tamoxifen

CCR2^{creERT2} x R26^{TdTomato} mice were treated with tamoxifen dissolved in corn oil (20 mg/mL) by a single oral gavage (250 μL/mouse). Animals were sacrificed 2 days later and assessed for labeling efficiency in brown adipose tissue by flow cytometry.

CX3CR1^{creERT2} x R26^{TdTomato} mice were injected intra-peritoneally with 10 mg/mL tamoxifen (200 μL per mouse in 10% EtOH and sunflower oil) daily for 5 days. Labelling efficiency was assessed in brain, blood and brown adipose tissue for each experiment involving this strain.

Ms4a3^{creERT2} x R26^{TdTomato} mice were treated with tamoxifen dissolved in corn oil (20 mg/mL) by oral gavage (100 μL/mouse) daily for 5 days. Labelling efficiency was assessed in blood and brown adipose tissue 3, 10 and 17 days following the last tamoxifen administration.

Monocyte depletion with MC-21

Mice were injected intra-peritoneally once a day for 1, 2 or 5 days with 10 μg MC-21 (anti-CCR2) antibody or vehicle (PBS) and were sacrificed 16 h after the last injection for analysis of brown adipose tissue macrophages. Monocyte depletion efficiency was confirmed by blood analysis.

Macrophage depletion with AFS98

Mice were injected intra-peritoneally twice (48 hours apart) with 500 μg anti-CD115 blocking antibody (AFS98, BioXCell cat#BE0213) or isotype control (Rat IgG2a, BioXcell cat#BE0089) and were sacrificed 16 h after the last injection for analysis of adipose tissue macrophages.

Flow cytometry

Tissues were harvested after cervical dislocation and washed in PBS. Splenocytes were prepared by gently crushing the spleen on a 70 μm strainer in flow buffer (PBS containing 1% BSA and 2 mM EDTA). Peritoneal cells were obtained by performing lavage with 5 mL flow buffer. Bone marrow cells were prepared by flushing femurs and tibias with flow buffer. Adipose tissues were harvested, minced with scissors, and then incubated for 45 min with PBS containing 3 mg/mL collagenase A at 37 °C. Digested adipose tissues were homogenized using a 1 mL syringe with a 20G needle and passed through a 100 μm strainer. Blood was drawn from the submandibular vein and collected in heparinized tubes or Eppendorf tubes containing 15 μl 500 mM EDTA. Red blood cells were lysed using BD Pharm Lyse lysing solution (BdBiosciences cat #555899). Cells were washed with flow buffer and then surface stained. All antibodies were used 1/200. A list of all antibodies used in provided in Supplementary Table 1. Flow cytometry data were acquired using a BD FACS Canto II and a Cytek Aurora cytometer with 5 laser configuration. All analyses were performed using FlowJo software (Tree Star).

Metabolite analyses

Colorimetric quantification of metabolites

Glycerol, TG and NEFA contents were measured from serum. Free glycerol reagent and standard were used according to the manufacturer's protocol. NEFA-HR2 R1 + R2 FUJIFILM were used according to the manufacturer's protocol.

Serum lipidomic analysis by GCMS-NCI

Materials: Fatty acid calibration standards and deuterated fatty acid internal standards (saturated and unsaturated) were purchased from CDN Isotopes (Cluzeau Info Lab, Sainte Foy La Grande, France) and Cayman (Bertin Pharma, Montigny-le-Bretonneux, France) respectively. Chemicals of the highest grade available were from Sigma Aldrich (Saint-Quentin Fallavier, France). LCMSMS quality grade solvents were purchased from Fischer Scientific (Illkirch, France).
Methods: Serum (25µL) was mixed with 5 µL of a fatty acid internal standard mix, containing 260 ng of myristic acid-d3, 1128 ng of palmitic acid-d3, 840 ng of stearic acid-d3, 720 ng of linoleic acid d4, 10.4 ng of arachidic acid-d3, 432 ng of arachidonic acid-d8, 10.8 ng of behenic acid-d3, 108 ng of DHA-d5, 5.2 ng of Lignoceric-d4, and 4 ng of cerotic acid-d4. To separate non-esterified fatty acids, the spiked serum samples were mixed with 1.2ml of Dole's reagent (Isopropanol/Hexane/Phosphoric acid 2M 40/10/1 v/v/v). Free fatty acids were then recovered with 1 ml of hexane and 1 ml of distilled water. The organic phase was collected and evaporated under vacuum. Fatty acids were then analyzed as pentafluorobenzyl esters (PFB-FAs esters) by NCI-GCMS as previously described (Nguyen et al., 2021). Calibration curves were obtained using myristic acid (0.05 - 0.8 µg), palmitic acid (1 - 8 µg), stearic acid (0.5 – 2 µg), linoleic acid (2 - 8 µg), arachidic acid (0.01 – 0.04 µg), arachidonic acid (1 - 4 µg), docosahexaenoic acid (0.4 – 1.6 µg), and docosapentaenoic acid (0.1 – 0.4 µg) extracted by the same method used for plasma. The abundances of serum free fatty acids were determined by negative chemical ionization mode (NCI) GCMS. Linear regression was applied for calculations.

Quantitative analysis of brown adipose tissues by targeted mass spectrometry
Materials: Glyceride standards, (17:0)2-d5 DG and (17:0)3 TG were obtained from Avanti Polar Lipids (Coger SAS, Paris, France). High-grade organic solvent modifiers were purchased from Sigma Aldrich (Saint-Quentin Fallavier, France). LC-MSMS quality grade solvents were purchased from Fischer Scientific (Illkirch, France).
Preparation of lipid extracts: Gravimetrically weighed adipose tissues suspended in $CHCl_3$:MeOH (2:1) were homogenized with the Omni Bead Ruptor 24 (Omni International. Inc.) coupled to a RT400 savant condensation trap (Thermo Scientific). DG (1µg) and TG (2.5µg) internal standards were added to approximately 0.5mg of adipose tissue homogenates. The spiked homogenates were vortexed, centrifuged, collected into inserts, dried under vacuum, and resuspended in 100µl of $CHCl_3$:MeOH (2:1).
Analysis of Glycerides by UHPLC-MS^2: The homogenates (3 µL) were analyzed by LC-MSMS. For the separation and elution of analytes, a Nucleodur ISIS C18 1,8 µm guard (3 x 4mm) and analytical (3 x 100mm) column (Marechey-Nagel, Hoerdt Cedex, France) maintained at 50°C were used(Tamba Sompila et al., 2017). Briefly, DG and TG were resolved on a 1260 Infinity LC system (Agilent Technologies) with a gradient of mobile phase A (acetonitrile/water/1M ammonium formate (60/39/1 v/v/v) with 0.1% formic acid), and mobile phase B (isopropanol/acetonitrile/1M ammonium formate (90/9/1 v/v/v) with 0.1% formic acid)(Cajka et al., 2023) at a flow rate of 0.45ml/min set as follows : 1 min hold at 30% B; 30-60% B in 2 min; 60-72% B in 15 min; 72-99% B in 20min; 3 min hold at 99%, 99%-30% ramp-down in 0.1 min and, maintained at 30% B for 3.9 min. Acquisition was realized on a 6460 Triple Quadrupole (Agilent Technologies) equipped with an ESI Jet stream source (temperature 150 °C, nebulizer 15 L/min, sheath gas 11 L/min, sheath gas temperature 150°C, capillary 4500 V and nozzle voltage 1200 V) operated in positive Single Reaction Monitoring (SRM) mode (fragmentor 152 and 220 V, collision energy 29 and 25 V for DG and TG

respectively. Ammoniated DG were quantified according to the response observed from the neutral loss of either their sn-1 or sn-2 fatty acid. Ammoniated TG were quantified according to the sum of the responses resulting from the neutral loss of either their sn-1, sn-2, and sn-3 fatty acids. Finally, lipid concentrations were determined by calculating the relative response of each lipiform to its respective internal standard.

Histology and immunostaining

Tissues were harvested and fixed in 4% paraformaldehyde solution for 4 h at room temperature or overnight at 4°C. First, a paraffin infiltration was performed on dehydrated tissues (Myr Spin Tissue Processor STP 120). Then, tissues were embedded in paraffin (inclusion center EC350-B&PMP). 7 µm sections were performed using a HM340E microtome (Microm Microtech, Francheville France). Paraffin sections were then de-paraffinized and stained using hematoxylin & eosin.

Transcriptomic analysis

Gene expression of MDP, GMP, LPM (MHC-II^{-} F4/80^{high}) and SPM (MHC-II^{+} F4/80^{low}) were retrived from Immgen dataset GSE15907 and analyzed using Phantasus (Kleverov et al., 2024). The signature from BAT CD226^{high} macrophages was isolated from our previously published single-cell RNA-sequencing dataset (GSE177635)(Gallerand et al., 2021) that can be explored at https://artyomovlab.wustl.edu/scn/?token=GSE177635

Single-cell RNA-seq integration

Single-cell datasets were downloaded from GEO database: GSE177635 (Gallerand et al., 2021) (brown fat tissue, WT sample GSM5378577); GSE203097 (Dolfi et al., 2022) (adrenal gland tissue, samples: GSM6153750 and GSM6153751); GSE225665 (Li et al., 2024) (peritoneal wash, samples: GSM7053956 and GSM7053957). For splenic tissue (Liu et al., 2023), single-cell dataset was downloaded from https://figshare.com/articles/dataset/Bulk_and_single-cell_RNA-seq_data/22232056/1. Cell type annotations were used from original studies (for brown fat and adrenal gland datasets - provided by authors, for peritoneal wash and spleen datasets downloaded together with data from public resources). Datasets were subsetted to maintain only monocyte, macrophage, and dendritic cell populations.

Datasets were integrated using Seurat v4.3.0 tool (Hao et al., 2021) using RPCA approach. Samples, coming from different datasets were log normalized, and 3000 variable features were selected using 'vst' method. After the selection of integration features, highly variable genes were scaled and variation coming from the percentage of mitochondrial genes and number of counts were regressed out. Integration anchors were found with no k.filter and 250 n.trees parameters. Integrated data were scaled and the final umap reduction was calculated based on the first 25 PCA components.

For DC3 signature enrichment, the top 100 differentially expressed genes were calculated using the FindMarkers function, with the following parameters: logfc.threshold = 0.01, min.pct = 0.01, only.pos = T. Enrichment plot was created using plotCoregulationProfileReduction function from fgsea package v1.27.1 (Korotkevich et al., 2021).

Scatter plots were visualized using ggplot2 v3.4.2 package (Wickham, 2016). Shapes of cluster borders were calculated by first estimating 2d kernel density using MASS package v7.3-58.4(Venables WN, 2002), followed by creating a grid graph with igraph package v1.4.3 (Csárdi G, 2024) and calculating α-shape of clusters using alphahull v2.5 package (Pateiro-

López, 2010). Visualization of gene expression for Gallerand et al., 2021 dataset in Figures S1, and S4 was generated using scNavigator (Artyomov lab, https://artyomovlab.wustl.edu/scn/).

Statistical Analysis

All data are represented in mean ± SEM. Statistical analysis was performed with GraphPad Prism 10 as indicated in each figure legend. Presence of statistically significant differences between conditions are indicated as follows: ns $p>0.05$; * $p<0.05$; ** $p<0.01$; *** $p<0.001$; **** $p<0.0001$.

References

Auffray, C., Fogg, D., Garfa, M., Elain, G., Join-Lambert, O., Kayal, S., Sarnacki, S., Cumano, A., Lauvau, G., and Geissmann, F. (2007). Monitoring of blood vessels and tissues by a population of monocytes with patrolling behavior. Science *317*, 666-670.

Cajka, T., Hricko, J., Rudl Kulhava, L., Paucova, M., Novakova, M., and Kuda, O. (2023). Optimization of Mobile Phase Modifiers for Fast LC-MS-Based Untargeted Metabolomics and Lipidomics. Int. J. Mol. Sci. *24*.

Carlin, L.M., Stamatiades, E.G., Auffray, C., Hanna, R.N., Glover, L., Vizcay-Barrena, G., Hedrick, C.C., Cook, H.T., Diebold, S., and Geissmann, F. (2013). Nr4a1-dependent Ly6C(low) monocytes monitor endothelial cells and orchestrate their disposal. Cell *153*, 362-375.

Cox, N., Crozet, L., Holtman, I.R., Loyher, P.L., Lazarov, T., White, J.B., Mass, E., Stanley, E.R., Elemento, O., Glass, C.K., and Geissmann, F. (2021). Diet-regulated production of PDGFcc by macrophages controls energy storage. Science *373*.

Croxford, A.L., Lanzinger, M., Hartmann, F.J., Schreiner, B., Mair, F., Pelczar, P., Clausen, B.E., Jung, S., Greter, M., and Becher, B. (2015). The Cytokine GM-CSF Drives the Inflammatory Signature of CCR2+ Monocytes and Licenses Autoimmunity. Immunity *43*, 502-514.

Csárdi G, N.T., Traag V, Horvát S, Zanini F, Noom D, Müller K (2024). igraph: Network Analysis and Visualization in R. *R package version 2.0.3*.

Dolfi, B., Gallerand, A., Firulyova, M.M., Xu, Y., Merlin, J., Dumont, A., Castiglione, A., Vaillant, N., Quemener, S., Gerke, H.*, et al.* (2022). Unravelling the sex-specific diversity and functions of adrenal gland macrophages. Cell Rep. *39*, 110949.

Gallerand, A., Stunault, M.I., Merlin, J., Luehmann, H.P., Sultan, D.H., Firulyova, M.M., Magnone, V., Khedher, N., Jalil, A., Dolfi, B.*, et al.* (2021). Brown adipose tissue monocytes support tissue expansion. Nat Commun *12*, 5255.

Gautier, E.L., Shay, T., Miller, J., Greter, M., Jakubzick, C., Ivanov, S., Helft, J., Chow, A., Elpek, K.G., Gordonov, S.*, et al.* (2012). Gene-expression profiles and transcriptional regulatory pathways that underlie the identity and diversity of mouse tissue macrophages. Nat Immunol *13*, 1118-1128.

Ginhoux, F., and Guilliams, M. (2016). Tissue-Resident Macrophage Ontogeny and Homeostasis. Immunity *44*, 439-449.

Han, J., Gallerand, A., Erlich, E.C., Helmink, B.A., Mair, I., Li, X., Eckhouse, S.R., Dimou, F.M., Shakhsheer, B.A., Phelps, H.M.*, et al.* (2024). Human serous cavity macrophages and dendritic cells possess counterparts in the mouse with a distinct distribution between species. Nat. Immunol. *25*, 155-165.

Hanna, R.N., Cekic, C., Sag, D., Tacke, R., Thomas, G.D., Nowyhed, H., Herrley, E., Rasquinha, N., McArdle, S., Wu, R.*, et al.* (2015). Patrolling monocytes control tumor metastasis to the lung. Science *350*, 985-990.
Hao, Y., Hao, S., Andersen-Nissen, E., Mauck, W.M., 3rd, Zheng, S., Butler, A., Lee, M.J., Wilk, A.J., Darby, C., Zager, M.*, et al.* (2021). Integrated analysis of multimodal single-cell data. Cell *184*, 3573-3587 e3529.
Ingersoll, M.A., Spanbroek, R., Lottaz, C., Gautier, E.L., Frankenberger, M., Hoffmann, R., Lang, R., Haniffa, M., Collin, M., Tacke, F.*, et al.* (2010). Comparison of gene expression profiles between human and mouse monocyte subsets. Blood *115*, e10-19.
Jung, S., Aliberti, J., Graemmel, P., Sunshine, M.J., Kreutzberg, G.W., Sher, A., and Littman, D.R. (2000). Analysis of fractalkine receptor CX(3)CR1 function by targeted deletion and green fluorescent protein reporter gene insertion. Mol Cell Biol *20*, 4106-4114.
Kim, K.W., Williams, J.W., Wang, Y.T., Ivanov, S., Gilfillan, S., Colonna, M., Virgin, H.W., Gautier, E.L., and Randolph, G.J. (2016). MHC II+ resident peritoneal and pleural macrophages rely on IRF4 for development from circulating monocytes. J Exp Med *213*, 1951-1959.
Kleverov, M., Zenkova, D., Kamenev, V., Sablina, M., Artyomov, M.N., and Sergushichev, A.A. (2024). Phantasus, a web application for visual and interactive gene expression analysis. Elife *13*.
Korotkevich, G., Sukhov, V., Budin, N., Shpak, B., Artyomov, M.N., and Sergushichev, A. (2021). Fast gene set enrichment analysis. bioRxiv, 060012.
Krljanac, B., Schubart, C., Naumann, R., Wirtz, S., Culemann, S., Kronke, G., and Voehringer, D. (2019). RELMalpha-expressing macrophages protect against fatal lung damage and reduce parasite burden during helminth infection. Sci Immunol *4*.
Li, X., Mara, A.B., Musial, S.C., Kolling, F.W., Gibbings, S.L., Gerebtsov, N., and Jakubzick, C.V. (2024). Coordinated chemokine expression defines macrophage subsets across tissues. Nat. Immunol. *25*, 1110-1122.
Liu, Z., Gu, Y., Chakarov, S., Bleriot, C., Kwok, I., Chen, X., Shin, A., Huang, W., Dress, R.J., Dutertre, C.A.*, et al.* (2019). Fate Mapping via Ms4a3-Expression History Traces Monocyte-Derived Cells. Cell *178*, 1509-1525 e1519.
Liu, Z., Wang, H., Li, Z., Dress, R.J., Zhu, Y., Zhang, S., De Feo, D., Kong, W.T., Cai, P., Shin, A.*, et al.* (2023). Dendritic cell type 3 arises from Ly6C(+) monocyte-dendritic cell progenitors. Immunity *56*, 1761-1777 e1766.
Mack, M., Cihak, J., Simonis, C., Luckow, B., Proudfoot, A.E., Plachy, J., Bruhl, H., Frink, M., Anders, H.J., Vielhauer, V.*, et al.* (2001). Expression and characterization of the chemokine receptors CCR2 and CCR5 in mice. J. Immunol. *166*, 4697-4704.
Mass, E., Nimmerjahn, F., Kierdorf, K., and Schlitzer, A. (2023). Tissue-specific macrophages: how they develop and choreograph tissue biology. Nat. Rev. Immunol. *23*, 563-579.
Menezes, S., Melandri, D., Anselmi, G., Perchet, T., Loschko, J., Dubrot, J., Patel, R., Gautier, E.L., Hugues, S., Longhi, M.P.*, et al.* (2016). The Heterogeneity of Ly6C(hi) Monocytes Controls Their Differentiation into iNOS(+) Macrophages or Monocyte-Derived Dendritic Cells. Immunity *45*, 1205-1218.
Miller, J.C., Brown, B.D., Shay, T., Gautier, E.L., Jojic, V., Cohain, A., Pandey, G., Leboeuf, M., Elpek, K.G., Helft, J.*, et al.* (2012). Deciphering the transcriptional network of the dendritic cell lineage. Nat Immunol *13*, 888-899.
Nguyen, M., Bourredjem, A., Piroth, L., Bouhemad, B., Jalil, A., Pallot, G., Le Guern, N., Thomas, C., Pilot, T., Bergas, V.*, et al.* (2021). High plasma concentration of non-esterified

polyunsaturated fatty acids is a specific feature of severe COVID-19 pneumonia. Sci. Rep. *11*, 10824.
Nicholls, D.G. (2017). The hunt for the molecular mechanism of brown fat thermogenesis. Biochimie *134*, 9-18.
Pateiro-López, B., & Rodríguez-Casal, A (2010). Generalizing the Convex Hull of a Sample: The R Package alphahull. Journal of Statistical Software *34(5), 1–28*.
Randolph, G.J., Ivanov, S., Zinselmeyer, B.H., and Scallan, J.P. (2017). The Lymphatic System: Integral Roles in Immunity. Annu. Rev. Immunol. *35*, 31-52.
Rosen, E.D., and Spiegelman, B.M. (2014). What we talk about when we talk about fat. Cell *156*, 20-44.
Schraml, B.U., van Blijswijk, J., Zelenay, S., Whitney, P.G., Filby, A., Acton, S.E., Rogers, N.C., Moncaut, N., Carvajal, J.J., and Reis e Sousa, C. (2013). Genetic tracing via DNGR-1 expression history defines dendritic cells as a hematopoietic lineage. Cell *154*, 843-858.
Serbina, N.V., and Pamer, E.G. (2006). Monocyte emigration from bone marrow during bacterial infection requires signals mediated by chemokine receptor CCR2. Nat. Immunol. *7*, 311-317.
Sunderkotter, C., Nikolic, T., Dillon, M.J., Van Rooijen, N., Stehling, M., Drevets, D.A., and Leenen, P.J. (2004). Subpopulations of mouse blood monocytes differ in maturation stage and inflammatory response. J Immunol *172*, 4410-4417.
Tabula Muris, C. (2020). A single-cell transcriptomic atlas characterizes ageing tissues in the mouse. Nature *583*, 590-595.
Tamba Sompila, A.W., Heron, S., Hmida, D., and Tchapla, A. (2017). Fast non-aqueous reversed-phase liquid chromatography separation of triacylglycerol regioisomers with isocratic mobile phase. Application to different oils and fats. J. Chromatogr. B Analyt. Technol. Biomed. Life Sci. *1041-1042*, 151-157.
Trzebanski, S., Kim, J.S., Larossi, N., Raanan, A., Kancheva, D., Bastos, J., Haddad, M., Solomon, A., Sivan, E., Aizik, D.*, et al.* (2024). Classical monocyte ontogeny dictates their functions and fates as tissue macrophages. Immunity.
Vanneste, D., Bai, Q., Hasan, S., Peng, W., Pirottin, D., Schyns, J., Marechal, P., Ruscitti, C., Meunier, M., Liu, Z.*, et al.* (2023). MafB-restricted local monocyte proliferation precedes lung interstitial macrophage differentiation. Nat Immunol *24*, 827-840.
Venables WN, R.B. (2002). Modern Applied Statistics with S, Fourth edition. Springer, New York *ISBN 0-387-95457-0*.
Wickham, H. (2016). ggplot2: Elegant Graphics for Data Analysis. Springer-Verlag New York *978-3-319-24277-4*.
Wolf, Y., Boura-Halfon, S., Cortese, N., Haimon, Z., Sar Shalom, H., Kuperman, Y., Kalchenko, V., Brandis, A., David, E., Segal-Hayoun, Y.*, et al.* (2017). Brown-adipose-tissue macrophages control tissue innervation and homeostatic energy expenditure. Nat Immunol *18*, 665-674.

Figure 1

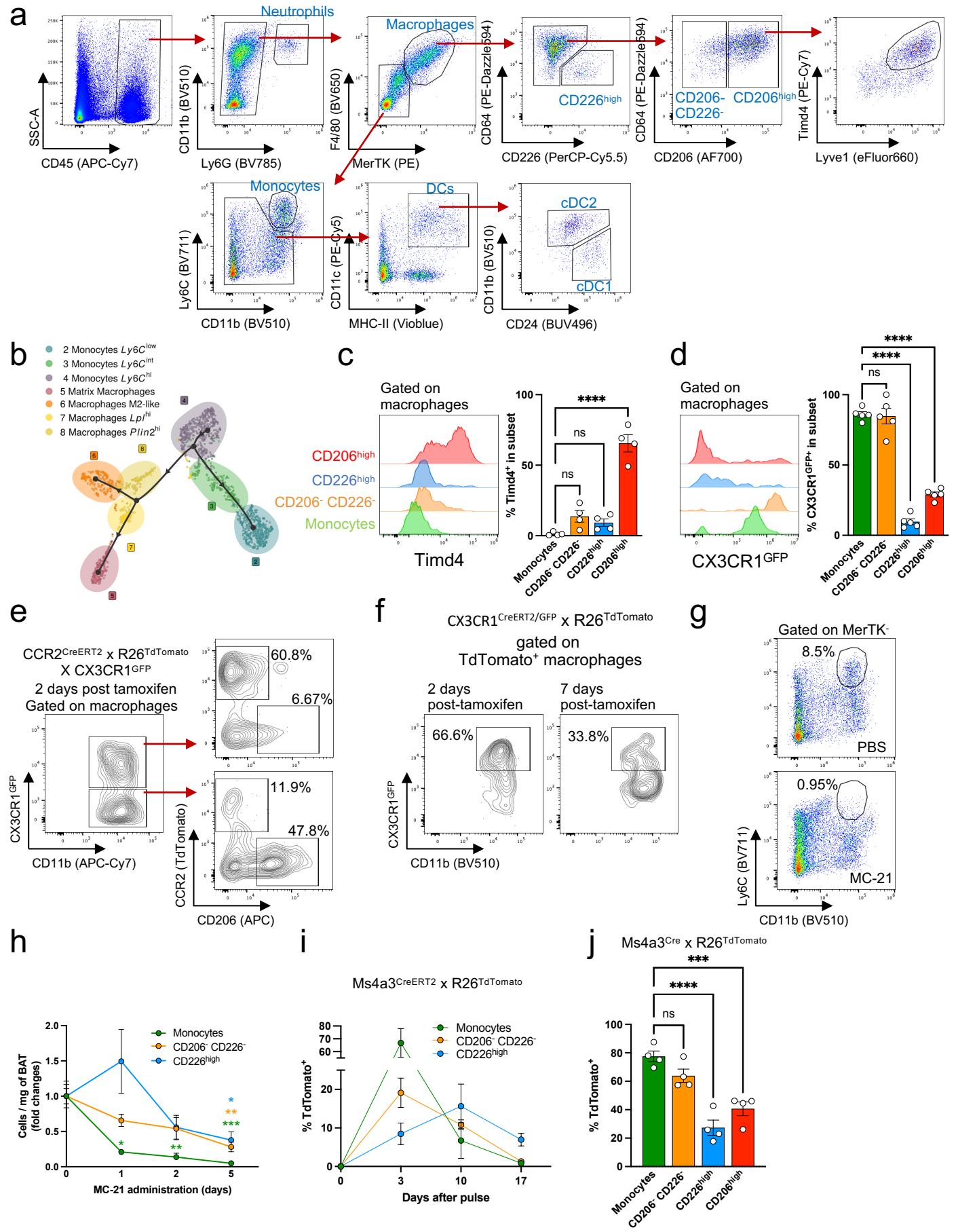
a
Neutrophils
Macrophages
Monocytes
DCs
cDC2
cDC1
SSC-A
CD45 (APC-Cy7)
CD11b (BV510)
Ly6G (BV785)
F4/80 (BV650)
MerTK (PE)
CD64 (PE-Dazzle594)
CD226 (PerCP-Cy5.5)
CD226high
CD206- CD226-
CD206 (AF700)
Timd4 (PE-Cy7)
Lyve1 (eFluor660)
Ly6C (BV711)
CD11c (PE-Cy5)
MHC-II (Violblue)
CD24 (BUV496)
b
2 Monocytes Ly6Clow
3 Monocytes Ly6Cint
4 Monocytes Ly6Chi
5 Matrix Macrophages
6 Macrophages M2-like
7 Macrophages Lpl hi
8 Macrophages Plin2hi
c
Gated on macrophages
CD206high
CD226high
CD206- CD226-
Monocytes
Timd4
% Timd4+ in subset
****
ns
d
Gated on macrophages
CX3CR1GFP
% CX3CR1GFP+ in subset
e
CCR2CreERT2 x R26TdTomato
X CX3CR1GFP
2 days post tamoxifen
Gated on macrophages
60.8%
6.67%
11.9%
47.8%
CX3CR1GFP
CD11b (APC-Cy7)
CCR2 (TdTomato)
CD206 (APC)
f
CX3CR1CreERT2/GFP x R26TdTomato
gated on
TdTomato+ macrophages
2 days
post-tamoxifen
7 days
post-tamoxifen
66.6%
33.8%
CX3CR1GFP
CD11b (BV510)
g
Gated on MerTK-
8.5%
PBS
0.95%
MC-21
Ly6C (BV711)
CD11b (BV510)
h
Monocytes
CD206- CD226-
CD226high
Cells / mg of BAT
(fold changes)
MC-21 administration (days)
i
Ms4a3CreERT2 x R26TdTomato
% TdTomato+
Days after pulse
j
Ms4a3Cre x R26TdTomato
% TdTomato+

Figure 1. Characterization of brown adipose tissue CD226^{high} macrophages.
(**a**) Gating strategy used to identify immune cell populations in adipose tissue. (**b**) Trajectory analysis of BAT myeloid cells using Slingshot. (**c, d**) Analysis of Timd4 (c) and CX3CR1^{GFP} (d) expression in BAT macrophages. (**e**) Fate mapping analysis of monocyte contribution to CX3CR1^{+} and CX3CR1^{-} BAT macrophages in CCR2^{CreERT2} x R26^{TdTomato} x CX3CR1^{GFP} mice that received tamoxifen gavage two days prior. (**f**) Fate mapping analysis of CX3CR1^{+} BAT macrophages using double reporter CX3CR1$^{CreERT2/GFP}$ x R26^{TdTomato} mice. (**g**) Validation of monocyte depletion in BAT from wild-type mice following MC-21 administration. (**h**) Time-course quantification of BAT macrophage subsets along MC-21 administration. (**i**) Time-course analysis of BAT monocyte and macrophage TdTomato labeling following tamoxifen administration in Ms4a3^{CreERT2} x R26^{TdTomato} mice. (**j**) Quantification of TdTomato^{+} cells among the indicated BAT monocyte and macrophage populations in Ms4a3^{Cre} x R26^{TdTomato} mice. Data are presented as mean values +/- SEM. See also Figures S1 and S2.

Figure 2

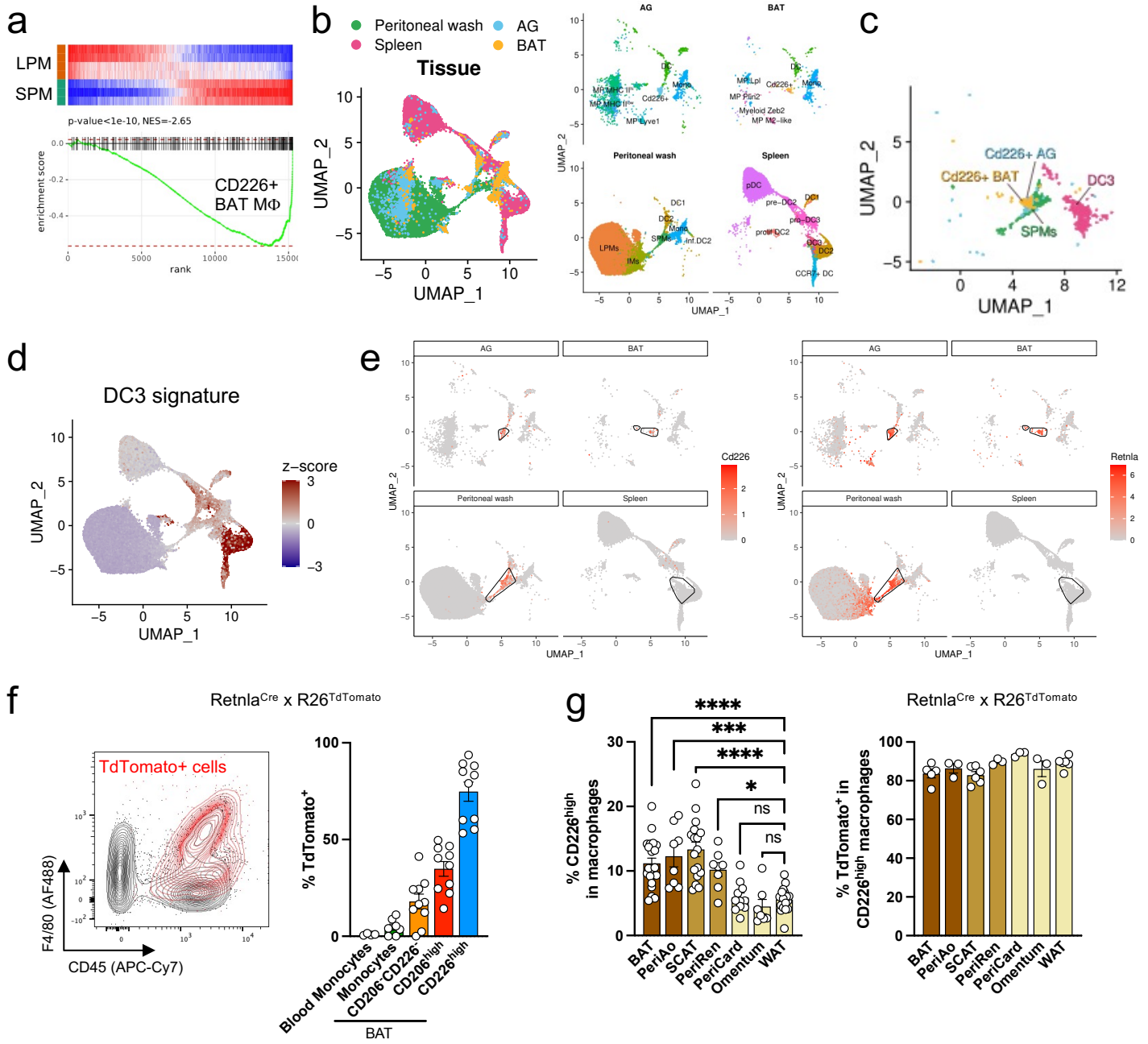

Figure 2. CD226^{high} macrophages are conserved across tissues and enriched in thermogenic adipose tissue.
(**a**) GSEA analysis, comparing the signature of BAT CD226^{high} macrophages to peritoneal LCMs and SCMs. (**b**) Single cell RNA-sequencing analysis of integrated datasets of immune cells from BAT, adrenal glands (AG) and peritoneal wash, and Flt3^{+} cells from spleen. (**c**) UMAP plot representing clustering of CD226^{+} macrophages from BAT, AGs and peritoneal wash, and DC3 from spleen. (**d**) UMAP plot representing expression of the DC3 signature by all cells contained in the integrated dataset from (b). (**e**) Expression of *Cd226* and *Retnla* by BAT, AG, peritoneal wash and spleen immune cells. (**f**) Flow cytometry plot showing distribution of TdTomato^{+} cells from Retnla^{cre} x R26^{TdT} mice in BAT (left) and quantification of TdTomato expression by blood and BAT monocytes and BAT macrophages (right). (**g**) Quantification of F4/80^{+} CD64^{low} CD226^{high} macrophages (left) and their expression of TdTomato in Retnla^{cre} x R26^{TdT} mice (right) in interscapular BAT, peri-aortic brown adipose tissue (PeriAo), subcutaneous adipose tissue (SCAT), peri-renal adipose tissue (PeriRen), peri-cardiac adipose tissue (PeriCard), omentum and gonadal white adipose tissue (WAT). Data are presented as mean values +/- SEM. See also Figure S3.

Figure 3

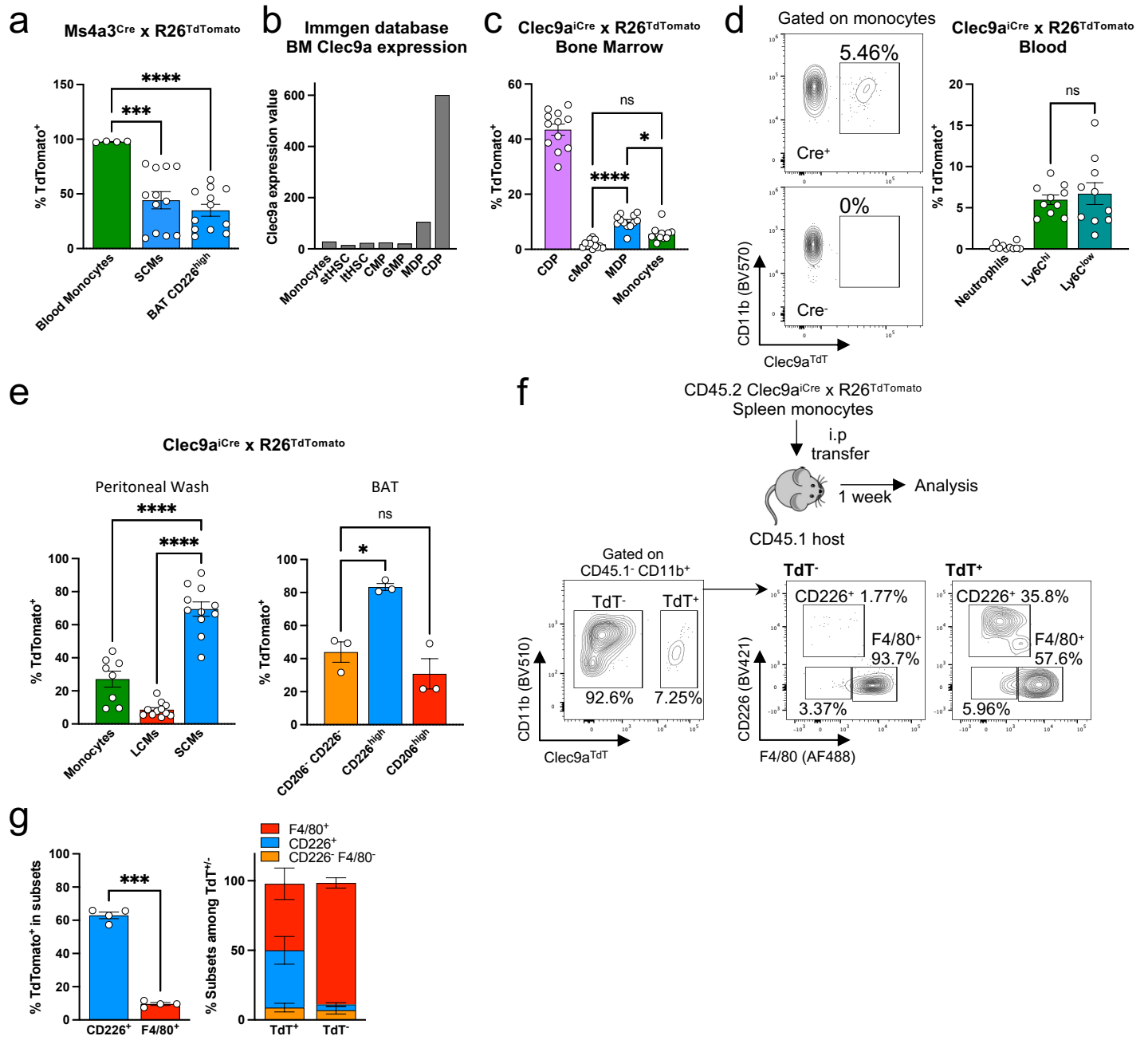

Figure 3. CD226^{high} macrophages develop from MDP-derived monocytes.
(**a**) Quantification of TdTomato^{+} cells among blood monocytes, peritoneal SCMs and BAT CD226^{high} macrophages in Ms4a3^{Cre} x R26^{TdT} mice. (**b**) Expression of *Clec9a* by bone marrow (BM) progenitors and monocytes. Data from Immgen.org. (**c**) Quantification of TdTomato^{+} cells among bone marrow progenitors and monocytes in Clec9a^{iCre} x R26^{TdT} mice. (**d**) Quantification of TdTomato^{+} cells among blood neutrophils and monocytes in Clec9a^{iCre} x R26^{TdT} mice. (**e**) Quantification of TdTomato^{+} cells among peritoneal and BAT monocytes and macrophages in Clec9a^{iCre} x R26^{TdT} mice. (**f**) Experimental design (top) and representative flow cytometry plots (bottom) showing phenotype of TdTomato^{+} and TdTomato^{-} monocytes from Clec9a^{iCre} x R26^{TdT} mice that were adoptively transferred intraperitoneally. (**g**) Quantification of TdTomato cells among peritoneal wash F4/80^{+} and CD226^{+} cells. Data are presented as mean values +/- SEM. See also Figure S4.

Figure 4

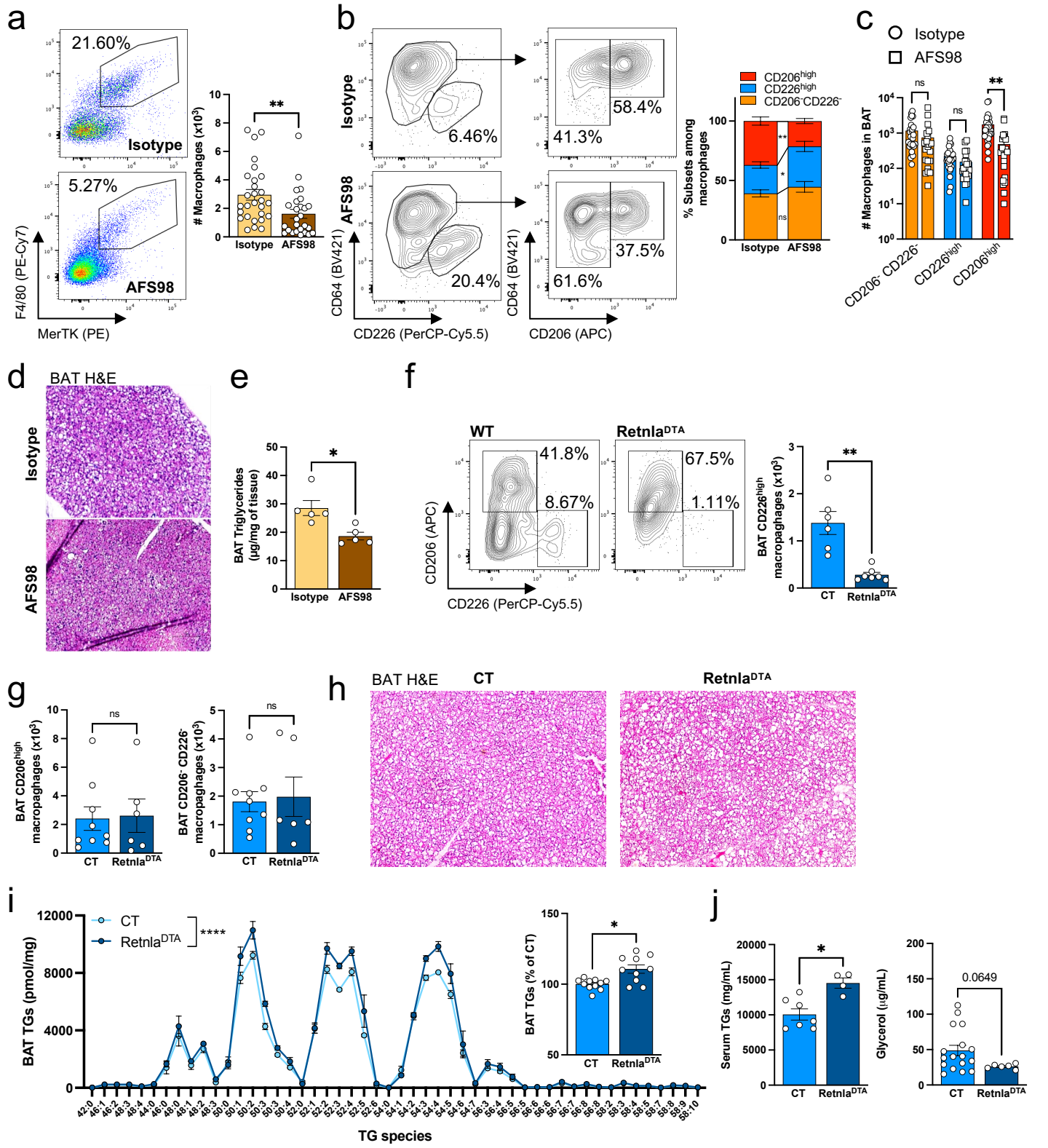

Figure 4. CD226^{high} macrophages regulate triglyceride metabolism.
(**a-c**) Representative flow cytometry plots and quantifications of total BAT macrophages (a) and BAT macrophage subsets (b and c) following CD115 blockade using AFS98. (**b**) Representative flow cytometry plot (left) and quantification (right) of BAT macrophage subsets following CD115 blockade using AFS98. (**d, e**) Hematoxylin and eosin staining of BAT (d) and quantification of BAT triglyceride content (e) following AFS98 treatment. (**f, g**) Representative flow cytometry plots (left) and quantification (right) of BAT CD226^{high} (f), CD206^{high} and CD206^{-} CD226^{-} (g) macrophages in Retnla^{Cre} x R26^{DTA} mice. (**h, i**) Hematoxylin and eosin staining of BAT (h) and triglyceride content analyzed using lipidomics (i) in Retnla^{Cre} x R26^{DTA} mice. (**j**) Quantification serum triglyceride (TG) and glycerol levels in Retnla^{Cre} x R26^{DTA} mice. Data are presented as mean values +/- SEM. See also Figure S5.